THREE-DIMENSIONAL EM MODELING

GERALD W. HOHMANN

Geology and Geophysics Department, University of Utah, Salt Lake City, Utah 84112, U.S.A.

Abstract. Three-dimensional (3D) interpretation of electromagnetic (EM) dsta is still in its infancy, due to a lack of practical numerical solutions for the forward problem. However, a number of algorithms for simulating the responses of simple 3D models have been developed over the last ten years, and they have provided important new insight. Integral equation methods have been more successful than differential equation methods, because they require calculating the electric field only in small anomalous regions, rather than throughout the earth. Utilizing a vector-scalar potential approach and incorporating symmetry through group theory improves the general 3D integral equation solution. Thin-sheet integral equation formulations have been particularly useful. Much recent research has focused on hybrid methods, which are finite element differential equation solutions within a mesh of limited extent, with boundary values determined by integrating over the interior fields. An elegant eigencurrent technique has been developed for calculating the transient response of a thin 3D sheet in free space, but general 3D time domain responses have only been calculated by Fourier transforming frequency domain results. Direct time domain calculations have been carried out only for 2D bodies.

1. Introduction

With the development of accurate, flexible, and reliable digital field instrumentation electromagnetic (EM) methods of geophysics now are limited mainly by a lack of interpretation capability. Layered earth (1D) interpretations often are used when they do not apply, because calculating the response of a 2D or 3D model requires a complicated numerical solution and a large amount of computer time and storage. Inversion techniques are well developed for 1D cases, but are very difficult to apply for 2D or 3D models. Thus in most cases interpretation of data must be accomplished by estimating the parameters of simplified 2D or 3D models of the earth using numerical solutions for forward calculations.

Differential equation (finite element and finite difference), integral equation, and hybrid methods have been used. Differential equation (DE) solutions are easiest to implement, and they result in large banded matrices. Because the entire earth is modeled on a grid, DE methods are preferable for simulating complex geology. Integral equation (IE) formulations involve more difficult mathematics, but the unknown fields only need to be found in anomalous regions. Thus IE solutions are less expensive for calculating the response of one or a few small bodies and hence are more useful for evaluating field techniques, for designing surveys, and for calculating interpretation catologs. Much recent research on 3D modeling has focused on hybrid methods, which attempt to combine the advantages of DE and IE solutions. Due to the numerous possibilities for theoretical and programming errors, it is necessary to compare results computed by different methods before a numerical solution can be considered valid. Too many results have been published without convergence checks and cross checks.

The subject of 3D EM interpretation is too large for a single review paper. I shall concentrate on reviewing the status of 3D numerical solutions, since further progress in

Geophysical Surveys **6** (1983) 27-53. 0046-5763/83/0061-0027$04.05.

this area is essential for improving EM methods of geophysics. Thus, I will not be able to treat scale modeling, which has provided much of our insight regarding 3D EM responses. Furthermore, it will be impossible to cover the various methods of 3D or quisi-3D interpretation of data, or inversion methods.

Theoretical formulations for total and secondary fields are derived in the first section, since they have not been presented in a unified manner before. Integral equation solutions, including a number of recent improvements, are considered next; they have been the most successful for 3D problems. Finite element and finite difference solutions are discussed next, followed by a section on hybrid methods. The final section discusses recent progress in time domain EM modeling. Checks between competing solutions are emphasized throughout, since validation is such an important aspect of numerical modeling.

2. Theoretical Formulations

Figure 1 shows a practical 3D model, consisting of an overburden layer of conductivity σ_1, a host rock of conductivity σ_2, a 3D body of variable conductivity $\sigma_b(\mathbf{r})$ imbedded in the host rock, and a basement of conductivity σ_3. Due to attenuation in the Earth, only low frequencies are of interst, so that displacement currents can be ignored. Furthermore, the effects of conductivity changes usually dominate those of magnetic permeability changes, so that we can set $\mu = \mu_0$ everywhere.

As illustrated in Figure 1, the source of the EM field can be either an impressed electric current $\mathbf{j}_p$ (a large loop or grounded wire) or a magnetic dipole with moment per unit volume $\mathbf{m}_p$ formed by a small loop of current.

2.1. Time domain equations

The coupled space and time dependence of the electric **e** and magnetic **h** fields is described by Maxwell's equations:

$$\nabla \times \mathbf{e}(\mathbf{r}, t) = -\mu_0 \frac{\partial \mathbf{h}(\mathbf{r}, t)}{\partial t} - \mu_0 \frac{\partial \mathbf{m}_p(\mathbf{r}, t)}{\partial t} \tag{1}$$

$$\nabla \times \mathbf{h}(\mathbf{r}, t) = \sigma \mathbf{e}(\mathbf{r}, t) + \mathbf{j}_p(\mathbf{r}, t). \tag{2}$$

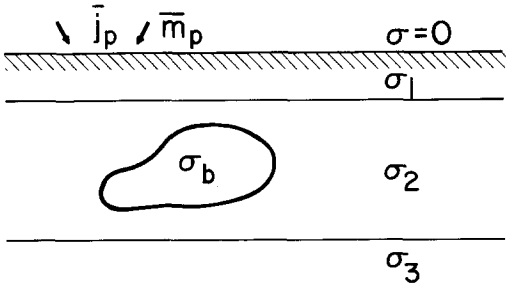

Fig. 1. Model of a 3D body in a layered earth.

Taking the curl of (1) and substituting (2), yields a vector diffusion equation for the electric field:

$$\nabla \times \nabla \times \mathbf{e} + \mu_0 \sigma \frac{\partial \mathbf{e}}{\partial t} = -\mu_0 \frac{\partial \mathbf{j}_p}{\partial t} - \mu_0 \nabla \times \frac{\partial \mathbf{m}_p}{\partial t}. \tag{3}$$

Similarly, taking the curl of (2) and substituting (1) yields a diffusion equation for the magnetic field:

$$\nabla \times \left(\frac{\nabla \times \mathbf{h}}{\sigma} \right) + \mu_0 \frac{\partial \mathbf{h}}{\partial t} = \nabla \times \left(\frac{\mathbf{j}_p}{\sigma} \right) - \mu_0 \frac{\partial \mathbf{m}_p}{\partial t}. \tag{4}$$

Equations (3) and (4) illustrate the important point that, due to attenuation in the Earth, EM methods of geophysics are based on a diffusion, rather than a wave, phenomenon. Hence, we cannot expect to achieve high resolution of structures at depth. Furthermore, the detailed shape of a body at depth is not important for numerical modeling.

We can write (3) as

$$-\nabla^2 \mathbf{e} + \nabla(\nabla \cdot \mathbf{e}) + \mu_0 \sigma \frac{\partial \mathbf{e}}{\partial t} = -\mu_0 \frac{\partial \mathbf{j}_p}{\partial t} - \mu_0 \nabla \times \frac{\partial \mathbf{m}_p}{\partial t}. \tag{5}$$

Taking the divergence of (2), we find:

$$\nabla \cdot (\sigma \mathbf{e}) = \sigma \nabla \cdot \mathbf{e} + \nabla \sigma \cdot \mathbf{e} = -\nabla \cdot \mathbf{j}_p.$$

Substituting for $\nabla \cdot \mathbf{e}$ in (5) yields

$$\nabla^2 \mathbf{e} + \nabla\left(\mathbf{e} \cdot \frac{\nabla \sigma}{\sigma} \right) - \mu_0 \sigma \frac{\partial \mathbf{e}}{\partial t} = \mu_0 \frac{\partial \mathbf{j}_p}{\partial t} - \frac{1}{\sigma} \nabla(\nabla \cdot \mathbf{j}_p) + \mu_0 \nabla \times \frac{\partial \mathbf{m}_p}{\partial t}, \tag{6}$$

assuming that the source is in a region of homogeneous conductivity.

Equation (4) can be rewritten as:

$$\frac{1}{\sigma} \nabla \times \nabla \times \mathbf{h} - \nabla \times \mathbf{h} \times \nabla\left(\frac{1}{\sigma} \right) + \mu_0 \frac{\partial \mathbf{h}}{\partial t} = \frac{1}{\sigma} \nabla \times \mathbf{j}_p - \mu_0 \frac{\partial \mathbf{m}_p}{\partial t},$$

or

$$-\nabla^2 \mathbf{h} + \nabla(\nabla \cdot \mathbf{h}) - \sigma \nabla \times \mathbf{h} \times \nabla\left(\frac{1}{\sigma} \right) + \mu_0 \sigma \frac{\partial \mathbf{h}}{\partial t} = \nabla \times \mathbf{j}_p - \mu_0 \sigma \frac{\partial \mathbf{m}_p}{\partial t}.$$

The divergence of the magnetic field is non-zero only at a magnetic source; taking the divergence of (1), we see that

$$\nabla \cdot \mathbf{h} = -\nabla \cdot \mathbf{m}_p.$$

Thus we finally obtain:

$$\nabla^2 \mathbf{h} + \sigma \nabla \times \mathbf{h} \times \nabla\left(\frac{1}{\sigma} \right) - \mu_0 \sigma \frac{\partial \mathbf{h}}{\partial t} = \mu_0 \sigma \frac{\partial \mathbf{m}_p}{\partial t} - \nabla(\nabla \cdot \mathbf{m}_p) - \nabla \times \mathbf{j}_p. \tag{7}$$

Equations (6) and (7) are general point equations for the total electric and magnetic fields, and they apply to the time-invariant case if the time derivatives are set to zero. Either of them can be solved numerically by time stepping, and then the other field can be calculated using (1) or (2). If, for example, only the magnetic field is desired, it would be advantageous to solve for it directly, since numerical differentiation introduces errors.

The primary fields, which would apply everywhere if the body were absent, satisfy the equations:

$$\nabla \times \mathbf{e}_p = -\mu_0 \frac{\partial \mathbf{h}_p}{\partial t} - \mu_0 \frac{\partial \mathbf{m}_p}{\partial t} \tag{8}$$

and

$$\nabla \times \mathbf{h}_p = \sigma_* \mathbf{e}_p + \mathbf{j}_p, \tag{9}$$

where σ_* is the 'normal' (layered-earth) conductivity with the body not present. These primary fields usually are in the form of integrals that can be evaluated numerically.

Subtracting (8) from (1) and (9) from (2) yields equations for the secondary fields:

$$\nabla \times \mathbf{e}_s = -\mu_0 \frac{\partial \mathbf{h}_s}{\partial t} \tag{10}$$

and

$$\nabla \times \mathbf{h}_s = \sigma \mathbf{e}_s + \sigma_a \mathbf{e}_p \tag{11a}$$

or

$$\nabla \times \mathbf{h}_s = \sigma_* \mathbf{e}_s + \mathbf{j}_s, \tag{11b}$$

where $\sigma_a = \sigma - \sigma_*$ is the anomalous conductivity at a point. In Figure 1 σ_a is non-zero only in the body, where it becomes $\sigma_a = \sigma_b - \sigma_*$. The quantity $\mathbf{j}_s$ is the equivalent (scattering) current that replaces the body and is the source of the secondary field; it is given by $\mathbf{j}_s = \sigma_a \mathbf{e}$.

Comparing (10) and (11a) with (1) and (2), we see that the DE for $\mathbf{e}_s$ is the same as that for $\mathbf{e}$ in (6), with the magnetic source terms deleted and with $\mathbf{j}_p$ replaced by $\sigma_a \mathbf{e}_p$:

$$\nabla^2 \mathbf{e}_s + \nabla\left(\mathbf{e}_s \cdot \frac{\nabla \sigma}{\sigma}\right) - \mu_0 \sigma \frac{\partial \mathbf{e}_s}{\partial t} = \mu_0 \sigma_a \frac{\partial \mathbf{e}_p}{\partial t} - \nabla\left(\mathbf{e}_p \cdot \frac{\nabla \sigma_a}{\sigma}\right), \tag{12}$$

since $\nabla \cdot \mathbf{e}_p$ is zero in the body, the only place where σ_a is not zero.

Similarly, the secondary magnetic field is given by modifying (7) in the same way:

$$\nabla^2 \mathbf{h}_s + \sigma \nabla \times \mathbf{h}_s \times \nabla\left(\frac{1}{\sigma}\right) - \mu_0 \sigma \frac{\partial \mathbf{h}_s}{\partial t} = -\sigma \nabla \times \left(\frac{\sigma_a}{\sigma} \mathbf{e}_p\right)$$

$$= -\sigma_a \nabla \times \mathbf{e}_p - \sigma \nabla\left(\frac{\sigma_a}{\sigma}\right) \times \mathbf{e}_p,$$

or, substituting (8)

$$\nabla^2 \mathbf{h}_s + \sigma \nabla \times \mathbf{h}_s \times \nabla\left(\frac{1}{\sigma}\right) - \mu_0 \sigma \frac{\partial \mathbf{h}_s}{\partial t} = \mu_0 \sigma_a \frac{\partial \mathbf{h}_p}{\partial t} - \sigma \nabla\left(\frac{\sigma_a}{\sigma}\right) \times \mathbf{e}_p, \tag{13}$$

since σ_a is zero at the position of the impressed magnetic source.

Notice that the sources of the secondary electric field in (12) are currents and charges in the volume on the surface of the body, where σ_a and $\nabla\sigma_a$ are non-zero. The sources of the secondary magnetic field in (13) are volume and surface currents in and on the body. The reasons for solving (12) and (13) rather than the equations for total fields are that they require fine spatial discretization only in the body, and that they permit the use of larger time steps, since the source is a smoother function of time.

2.2. Frequency domain equations

To obtain equations in the frequency domain, we perform a Fourier transformation, using the pair

$$\mathbf{F}(\mathbf{r}, \omega) = \int_{-\infty}^{\infty} \mathbf{f}(\mathbf{r}, t)\, e^{-i\omega t}\, \mathrm{d}t \tag{14a}$$

$$\mathbf{f}(\mathbf{r}, t) = \frac{1}{2\pi} \int_{-\infty}^{\infty} \mathbf{F}(\mathbf{r}, \omega)\, e^{i\omega t}\, \mathrm{d}\omega, \tag{14b}$$

which amounts to assuming an $e^{i\omega t}$ time dependence. Then (6) becomes

$$\nabla^2\mathbf{E} + \nabla\left(\mathbf{E} \cdot \frac{\nabla\sigma}{\sigma}\right) + k^2\mathbf{E} = i\omega\mu_0\mathbf{J}_p - \frac{1}{\sigma}\nabla(\nabla \cdot \mathbf{J}_p) + i\omega\mu_0\nabla \times \mathbf{M}_p. \tag{15}$$

From (7) we have

$$\nabla^2\mathbf{H} + \sigma\nabla \times \mathbf{H} \times \nabla\left(\frac{1}{\sigma}\right) + k^2\mathbf{H} = i\omega\mu_0\sigma\mathbf{M}_p - \nabla(\nabla \cdot \mathbf{M}_p) - \nabla \times \mathbf{J}_p, \tag{16}$$

while from (12)

$$\nabla^2\mathbf{E}_s + \nabla\left(\mathbf{E}_s \cdot \frac{\nabla\sigma}{\sigma}\right) + k^2\mathbf{E}_s = -k_a^2\mathbf{E}_p - \nabla\left(\mathbf{E}_p \cdot \frac{\nabla\sigma_a}{\sigma}\right). \tag{17}$$

Finally, from (13)

$$\nabla^2\mathbf{H}_s + \sigma\nabla \times \mathbf{H}_s \times \nabla\left(\frac{1}{\sigma}\right) + k^2\mathbf{H}_s = -k_a^2\mathbf{H}_p - \sigma\nabla\left(\frac{\sigma_a}{\sigma}\right) \times \mathbf{E}_p, \tag{18}$$

with

$$k^2 = -i\omega\mu_0\sigma,$$

and

$$k_a^2 = -i\omega\mu_0\sigma_a.$$

Equations (15)–(18) are the differential equations to be solved for the total and secondary electric and magnetic fields in the frequency domain. In the case of total fields, away from sources the other component can be found using the frequency

domain versions of (1) and (2):

$$\nabla \times \mathbf{E} = -i\omega\mu_0\mathbf{H} \tag{19}$$

$$\nabla \times \mathbf{H} = \sigma\mathbf{E}. \tag{20}$$

For secondary field solutions the other component can be calculated using the frequency domain versions of (10) and (11b):

$$\nabla \times \mathbf{E}_s = -i\omega\mu_0\mathbf{H}_s \tag{21}$$

$$\nabla \times \mathbf{H}_s = \sigma_* \mathbf{E}_s + \mathbf{J}_s. \tag{22}$$

To formulate an integral equation, we treat $\mathbf{J}_s$ in (22) as a source current. In a whole space the secondary electric field would be given by

$$\mathbf{E}_s = -i\omega\mu_0\mathbf{A} - \nabla\varphi, \tag{23}$$

where $\mathbf{A}$ and φ are vector scalar potentials for the Lorentz gauge, given by

$$\mathbf{A}(\mathbf{r}) = \int_v \mathbf{J}_s(\mathbf{r}')\, G(\mathbf{r}, \mathbf{r}')\, \mathrm{d}v', \tag{24}$$

and

$$\varphi(\mathbf{r}) = -\frac{1}{\sigma_*}\int_v \nabla \cdot \mathbf{J}_s(\mathbf{r}')\, G(\mathbf{r}, \mathbf{r}')\, \mathrm{d}v', \tag{25}$$

where G is the scalar EM Green's function:

$$G(\mathbf{r}, \mathbf{r}') = \frac{e^{-ik_*|\mathbf{r}-\mathbf{r}'|}}{4\pi|\mathbf{r} - \mathbf{r}'|} \tag{26}$$

For a body in a half space, an additional term, given by Wannamaker and Hohmann (1983), must be added to (23) to account for the layering. Thus the secondary field is due to currents and charges; the charges occur at discontinuities in $\mathbf{J}_s = \sigma_a\mathbf{E}$.

By adding the primary field to (23) we get a singular Fredholm integral equation of the second kind for the total electric field, which we can write as:

$$\mathbf{E}(\mathbf{r}) = \mathbf{E}_p(\mathbf{r}) + \int_v \mathscr{G}(\mathbf{r}, \mathbf{r}') \cdot \mathbf{E}(\mathbf{r}') \cdot \mathbf{E}(\mathbf{r}')\sigma_a(\mathbf{r}')\, \mathrm{d}v', \tag{27}$$

where $\mathscr{G}$ is the half-space dyadic Green's function. (Wannamaker and Hohmann, 1983)

2.3. Numerical solutions

All numerical solutions in the frequency domain and numerical solutions for the spatial dependence in the time domain can be placed in the context of the method of moments (Harrington, 1968), also called the method of weighted residuals or the Bubnov-Galerkin method. The spatial variation of any of the equations derived above can be written

$$Lf = g, \tag{28}$$

where L is a differential or integral operator, f is an unknown field, and g is a source term.

Approximating f by an N-term sum of suitably chosen expansion functions,

$$\hat{f}(\mathbf{r}) = \sum_{n=1}^{N} a_n f_n(\mathbf{r}), \tag{29}$$

are substituting in (28), we obtain

$$\sum_{n=1}^{N} a_n L f_n + \varepsilon = g, \tag{30}$$

where $\varepsilon(\mathbf{r})$ is the error of approximation.

Next we define a set of N weight functions, $w_m(\mathbf{r})$ and a suitable inner product, which is just an integral over some volume in the Earth. Then we take the inner product of (30) with each w_m:

$$\sum_{n=1}^{N} a_n \langle w_m, Lf_n \rangle + \langle w_m, \varepsilon \rangle = \langle w_m, g \rangle, \tag{31}$$

$$m = 1, 2, \ldots, N.$$

Requiring $\langle w_m, \varepsilon \rangle = 0$ for all m forces the error to be orthogonal to the weight functions, and (31) becomes

$$\sum_{n=1}^{N} a_n \langle w_m, Lf_n \rangle = \langle w_m, g \rangle, \tag{32}$$

which defines a matrix equation

$$\mathbf{Za} = \mathbf{g}, \tag{33}$$

with

$$z_{mn} = \langle w_m, Lf_n \rangle,$$

and

$$g_m = \langle w_m, g \rangle$$

to be solved for $\mathbf{a}$, the vector of unknown coefficients. Then $\hat{f}$, the approximation for f, is given by (29).

Pulse expansion functions, resulting in a step approximation, and delta weight functions generally are used for IE solutions in geophysical EM problems. Finite difference methods approximate the operator, as discussed by Harrington (1968). Finite element methods generally utilize the same linear, subdomain expansion and weight functions. For example, for tetrahedral subdomain elements, the nth expansion function for a linear approximation can be written (Pridmore *et al.*, 1981)

$$f_n(x, y, z) = a_n^1 + a_n^2 x + a_n^3 y + a_n^4 z. \tag{34}$$

In the finite element method the expansion function is rewritten in terms of the nodal values f_n^i, i.e.,

$$f_n(x, y, z) = f_n^1 N_1(x, y, z) + f_n^2 N_2(x, y, z) + f_n^3 N_3(x, y, z) + \\ + f_n^4 N_4(x, y, z), \tag{35}$$

where the N_i are termed 'shape functions'.

The finite element method seems to be a little better than the finite difference method for EM problems in geophysics, because it can handle abrupt and sloping conductivity interfaces with greater ease. Elaborate procedures are required to derive valid finite-difference approximations at conductivity boundaries (Jones and Thompson, 1974; Brewitt-Taylor and Weaver, 1976).

3. Integral Equation Solutions

Integral equation methods have been more successful than differential equation methods for 3D modeling, because it is only necessary to calculate the electric field in small anomalous regions rather than throughout the earth. Three dimensional DE grids quickly become unmanageable.

Numerical results obtained by solving (27) using pulse basis and delta weight functions, were first published by Hohmann (1975) and by Weidelt (1975). A prismatic body is divided into N cubic cells of dimension Δ and the scattering current, $\mathbf{J}_s = \sigma_a \mathbf{E}$, is assumed constant in each cell. Then the integral equation is approximated by the finite summation

$$\mathbf{E}(\mathbf{r}) = \mathbf{E}_p(\mathbf{r}) + \sum_{n=1}^{N} \int_{v_n} dv' \mathscr{G}(\mathbf{r}, \mathbf{r}') \cdot \mathbf{J}_s^n. \tag{36}$$

The primary field $\mathbf{E}_p$ is just the layered earth field that would be present at $\mathbf{r}$ if there were no inhomogeneity. It is found by evaluating Hankel transform integrals numerically.

The integration over the dyadic Green's function can be carried out numerically (Meyer, 1976) or analytically over the volumes and surfaces of the cells (Hohmann, 1975) to obtain the equation

$$\frac{1}{\sigma_a} \mathbf{J}_s(\mathbf{r}) = \mathbf{E}_p(\mathbf{r}) + \sum_{n=1}^{N} \Gamma(\mathbf{r}, \mathbf{r}_n) \cdot \mathbf{J}_s^n, \tag{37}$$

where $\mathbf{J}_s^n$ is the polarization current in cell n, and Γ is the dyadic Green's function for a small volume of current, unlike $\mathscr{G}$, which applies to an infinitesimal current element. Care must be taken in deriving Γ, because $\mathscr{G}$ is singular at $\mathbf{r} = \mathbf{r}'$.

To improve the solution, we now derive (37) in a manner similar to that described by Hohmann (1975), except that, following Harrington (1968), we approximate the derivatives of the scalar potential in (23) with differences. Also, instead of concentrating the charge (the $\nabla \cdot \mathbf{J}_s$ term in (25)) at the boundaries between cells, we distribute it

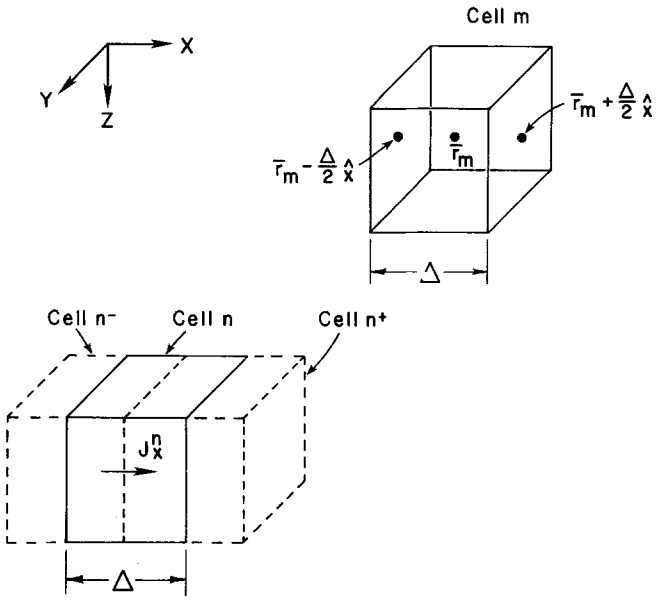

Fig. 2. Illustration of geometry for calculating the matrix element Z_{xx}^{mn}.

uniformly over a volume extending from the center of one cell to the center of the next cell. As various authors have indicated, approximating derivatives with differences provides accuracy similar to that of higher-order basis functions but is much easier to implement on a computer. See, e.g., Miller and Deadrick (1975), and Butler and Wilton (1975).

Figure 2 illustrates the calculation of the x component of secondary electric field at the center of cell m due to the x component of current in cell n. If we denote the center of cell m as $\mathbf{r}_m$, the x component of the vector potential from (24) becomes

$$A_x^{mn} = A_x(\mathbf{r}_m) = J_x{}^n \int_n G(\mathbf{r}_m, \mathbf{r}')\, dv', \tag{38}$$

which is the volume current contribution.

The charge contribution to the electric field is derived from the scalar potential in (25). The derivative at the current discontinuity between cell n and cell $n+1$ is approximated by

$$\frac{\partial J_x}{\partial x} \approx \frac{J_x^{n+1} - J_x{}^n}{\Delta}, \tag{39}$$

and is distributed uniformly in a cubic cell, denoted n^+ in Figure 2, extending from the center of cell n to the center of cell $n+1$. The charge at the other end of cell n is similarly distributed over cell n^-. Then the potentials φ_{x+}^{mn} and φ_{x-}^{mn} at points $\mathbf{r}_m + (\Delta/2)\hat{\mathbf{x}}$ and $\mathbf{r}_m - (\Delta/2)\hat{\mathbf{x}}$ due to $J_x{}^n$ are given by (25), which becomes

$$\varphi_{x+}^{mn} = \frac{J_x{}^n}{\sigma_* \Delta}\left[- \int_{n^-} G\left(\mathbf{r}_m + \frac{\Delta}{2}\hat{\mathbf{x}}, \mathbf{r}'\right) dv' + \int_{n^+} G\left(\mathbf{r}_m + \frac{\Delta}{2}\hat{\mathbf{x}}, \mathbf{r}'\right) dv' \right] \tag{40}$$

and

$$\varphi_{x-}^{mn} = \frac{J_x{}^n}{\sigma_* \Delta}\left[- \int_{n^-} G\left(\mathbf{r}_m - \frac{\Delta}{2}\hat{\mathbf{x}}, \mathbf{r}'\right) dv' + \int_{n^+} G\left(\mathbf{r}_m - \frac{\Delta}{2}\hat{\mathbf{x}}, \mathbf{r}'\right) dv' \right]. \tag{41}$$

Finally, E_{xs}^{mn} is given by (23), which becomes

$$E_{xs}^{mn} = -i\omega\mu_0 A_x^{mn} - (\varphi_{x+}^{mn} - \varphi_{x-}^{mn})/\Delta. \tag{42}$$

In terms of the method of moments, this solution is equivalent to using pulse functions for both current and charge and approximating the operator. To obtain Γ in (37), we need to evaluate the integrals in (38), (40), and (41) for each cartesian component of current. The integrals all have the same form: the scalar Green's function integrated over a cubic cell.

We can write Γ as the sum of two components representing current and charge sources:

$$\Gamma = \Gamma_A + \Gamma_\varphi, \tag{43}$$

where, for illustration, the x component of secondary electric field at the center of cell m due to the x component of scattering current in cell n is given by

$$E_{xs}^{mn} = [\Gamma_A^{xx,mn} + \Gamma_\varphi^{xx,mn}] J_x{}^n. \tag{44}$$

From (38) and (42), we see that

$$\Gamma_A^{xx,mn} = -i\omega\mu_0 \int_n G(\mathbf{r}_m, \mathbf{r}')\, dv', \tag{45}$$

while from (40), (41), and (42), we have

$$\Gamma_\varphi^{xx,mn} = -\frac{1}{\sigma_* \Delta}\left[- \int_{n^-} G\left(\mathbf{r}_m + \frac{\Delta}{2}\hat{\mathbf{x}}, \mathbf{r}'\right) dv' + \int_{n^+} G\left(\mathbf{r}_m + \frac{\Delta}{2}\hat{\mathbf{x}}, \mathbf{r}'\right) dv' - \right.$$
$$\left. \int_{n^-} G\left(\mathbf{r}_m - \frac{\Delta}{2}\hat{\mathbf{x}}, \mathbf{r}'\right) dv' + \int_{n^+} G\left(\mathbf{r}_m - \frac{\Delta}{2}\hat{\mathbf{x}}, \mathbf{r}'\right) dv' \right]. \tag{46}$$

The other elements of the dyadic Green's function can be derived by analogy.

For our case of a body in the Earth we divide Γ_A and Γ_φ into primary and secondary parts, where the secondary parts account for the earth-air interface and any other layers, as described by Hohmann (1975) and Wannamaker and Hohmann (1983).

The integrals in (45) and (46) only need to be evaluated for the primary parts of the Green's function, and they all have the same form:

$$I = \int_v \frac{e^{-ik_*|\mathbf{r}_m - \mathbf{r}'|}}{4\pi|\mathbf{r}_m - \mathbf{r}'|} \mathrm{d}v'. \tag{47}$$

The shape of the cell is not important for this volume integration, so we can replace the cube by a sphere of the same volume and integrate analytically as described by Hohmann (1975).

In more concise notation, (37) becomes

$$\frac{1}{\sigma_a}\mathbf{J}_s{}^m = \mathbf{E}_p{}^m + \sum_{n=1}^{N} \Gamma_{mn} \cdot \mathbf{J}_s{}^n, \tag{48}$$

where $\mathbf{J}_s{}^m$ and $\mathbf{J}_s{}^n$ are the scattering currents in cells m and n, respectively.

Rearranging (48) yields

$$\sum_{n=1}^{N} \left[\Gamma_{mn} - \frac{1}{\sigma_a}\delta_{mn} \right] \cdot \mathbf{J}_s{}^n = -\mathbf{E}_p{}^m, \tag{49}$$

in which

$$\delta_{mn} = \begin{cases} \mathscr{I}, m = n \\ \mathscr{O}, m \neq n, \end{cases}$$

where $\mathscr{I}$ is the unit dyadic and $\mathscr{O}$ is the null dyadic.

Writing (49) for each of the N values of m yields a partitioned matrix equation

$$\mathbf{Z} \cdot \mathbf{J}_s = -\mathbf{E}_p, \tag{50}$$

to solve for the polarization current in the body. The elements of the impedance matrix $\mathbf{Z}$ are themselves 3×3 matrices, given by

$$\mathbf{Z}_{mn} = \Gamma_{mn} - \frac{1}{\sigma_a}\delta_{mn}. \tag{51}$$

Figure 3 shows the improvement in the 3D integral equation resulting from distributing the charge over a volume rather than concentrating it on the surface of a cell, and from approximating the derivative of the scalar potential by a difference. The source is a plane wave at 1 Hz, with electric field normal to the long axis of a prismatic conductor, so the response is primarily due to current channeling. Since the effects of the ends of the body are small for this source polarization, near the body the 3D results should be close to the 2D profile shown. Note the much improved agreement for the new formulation.

The impedance matrix is full, with dimension $3N \times 3N$, where N is the number of cells into which the body is divided. Because the cell size must be less than a skin depth in the body and less than the depth to the top of the cell, matrix computation time and storage can be excessive. However, as Tripp and Hohmann (1983) show, the impedance matrix for a body with two vertical symmetry planes can be block diagonalized using group theory. The similarity transformation that block diagonalizes $\mathbf{Z}$ is the same as

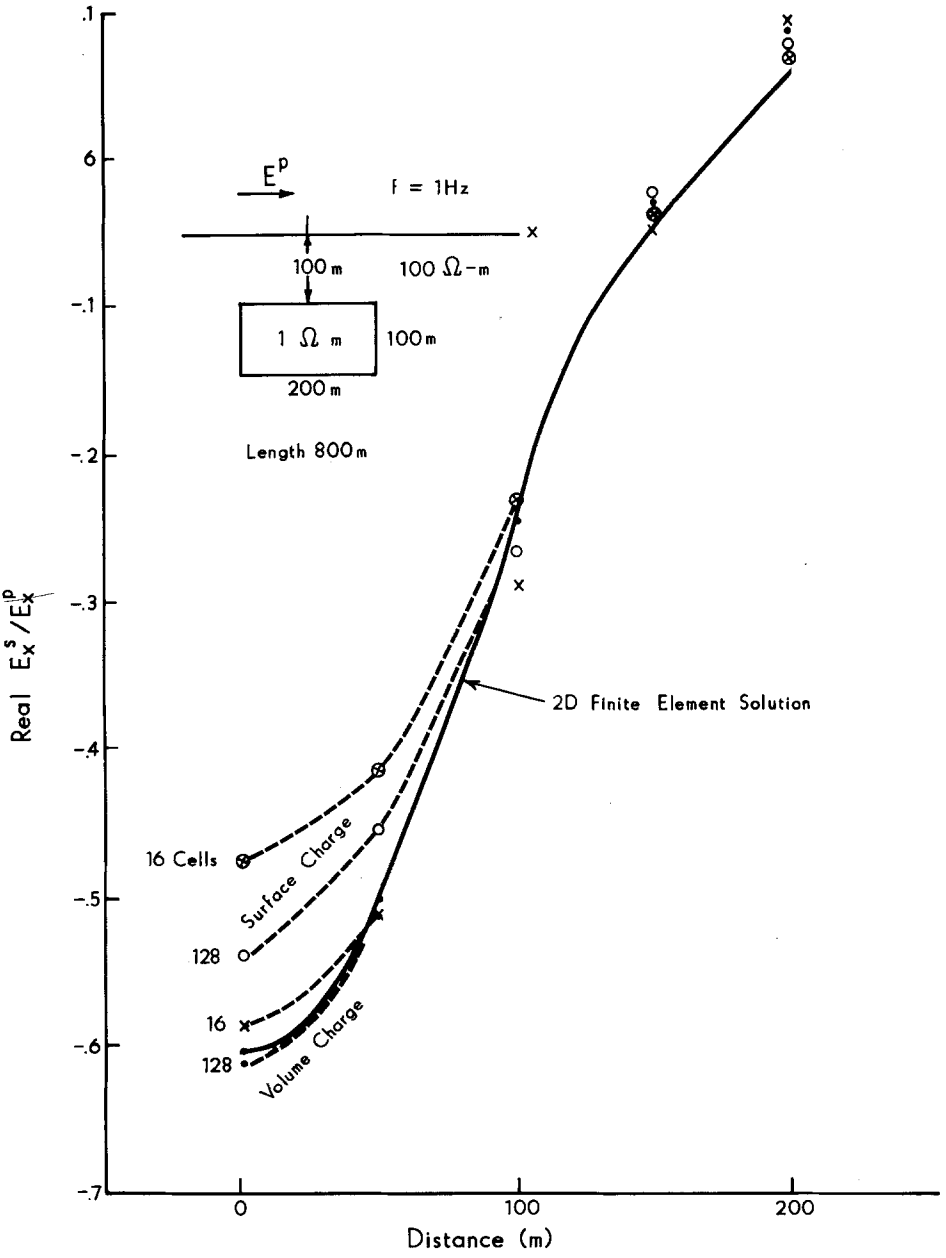

Fig. 3. Improvement in 3D integral equation solution resulting from using a vector-scalar potential formulation for the secondary field.

the one that diagonalizes the group representation matrices $\mathbf{R}$. The diagonalized matrix $\mathbf{R}'$ is given by

$$\mathbf{R}' = \mathbf{U}\mathbf{R}\mathbf{U}^T, \tag{52}$$

where $\mathbf{U}$ is easily derived using group theory. Then the block diagonalized impedance matrix is given by

$$\mathbf{Z}' = \mathbf{U}\mathbf{Z}\mathbf{U}^T. \tag{53}$$

In the new basis, the scattering problem becomes

$$\mathbf{Z}'\mathbf{J}_s' = -\mathbf{E}_p', \tag{54}$$

which is much easier to solve than (50). The scattering current in the original basis is given by back transforming:

$$\mathbf{J}_s = \mathbf{U}^T\mathbf{J}_s'. \tag{55}$$

Since the basis transformation is inexpensive, this procedure is superior to a direct solution.

The block diagonalized impedance matrix is composed of four sub-matrices, each with dimension $(3N/4) \times (3N/4)$. Thus the transformed matrix requires only a fourth of the storage required by the original matrix. The number of operations required for inversion is smaller by a factor of 12. Because it is only necessary to store one of the four sub-matrices in core at a time, core storage is reduced by a factor of 16. Matrix formation time for a symmetric body, including the similarity transformation, is about one third of that for a general body. A symmetric 3D body is a very useful geophysical model; these savings are significant, because they result in greater accuracy and/or greatly reduced computation costs.

In many cases the IE solution can be improved further by subdividing the body into rectangular prisms rather than cubes, as discussed by Wannamaker and Hohmann (1983). Modifying the basic solution is simple, since the integration over a prism can be treated as a summation over cubic sub-cells. Rectangular cells are useful for approximating an elongated body, because the scattering current varies more rapidly in the short direction of the body.

Figure 4 illustrates such a case and shows the accuracy that can be obtained for a purely inductive response. The source is a plane wave with the electric field in the long direction of the body, which has a conductivity contrast of 1000 with its half-space host. Since the body is about 10 skin depths (in the host) long, the 3D results should be the same as those for a 2D body of the same cross section. The 2D and 3D horizontal magnetic field results for a profile over the center of the body shown in Figure 4 are in good agreement, particularly for the finer discretization. The finer discretization consisted of 168 cells (504 unknowns) per quadrant of the body in plan view, and the results were computed in about 70 hr on a Prime 400 computer, while the coarser discretization required only 7 hr.

A major unsolved problem with the integral equation technique, at least for controlled-source applications, arises from the disparity in sizes of the current and charge terms in (43) for low but non-negligible host conductivity. The important information contributed by the induction operator Γ_A seems to be lost when the two terms are added. Lajoie and West (1976) avoided this problem by solving for curl-free

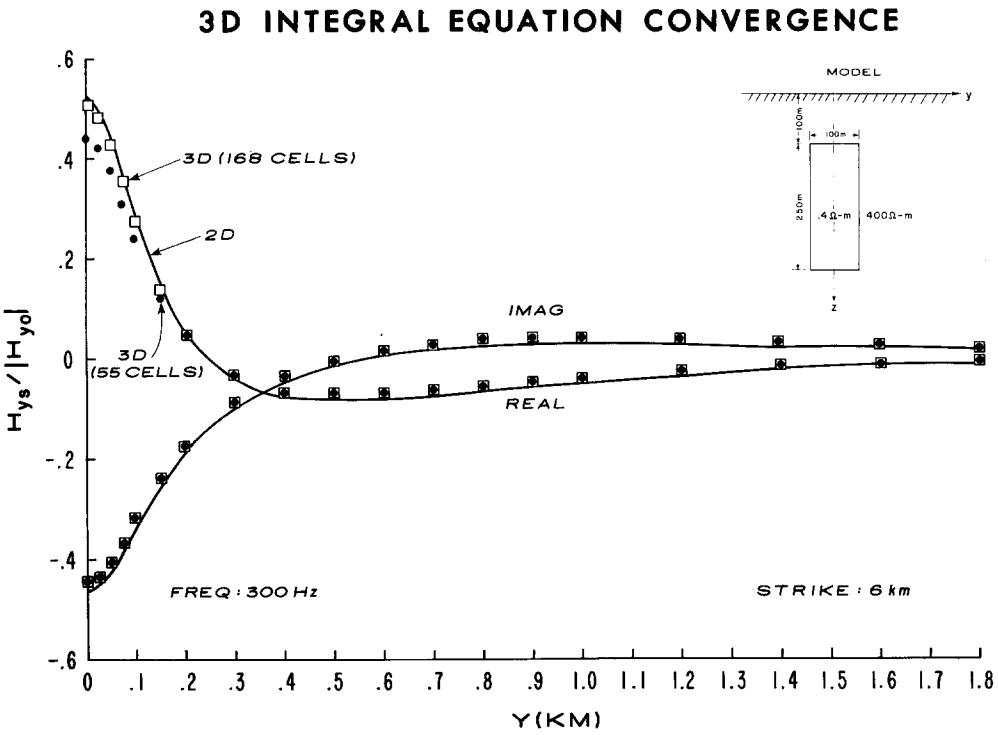

Fig. 4. Comparison between 2D finite element results and 3D integral equation results with two discretizations. The source is a plane wave with electric field in the x direction.

and divergence-free scattering currents on a thin 3D plate in a conductive half space. Their results provided important new insight into EM responses of 3D bodies. Understanding the relation between current channeling and induction, based largely on their work, has been a major breakthrough in EM applications. Figure 5 shows a typical result from their work. The model is a 3D plate in a conductive half-space excited by a large source loop. Even with a half-space resistivity as high as 3000 ohm-m, the response is quite different from the free-space ($\rho = \infty$) response. As the half-space resistivity decreases, the EM response of the plate changes completely, with the imaginary part changing sign at 200 ohm-m.

Dawson and Weaver (1979) discussed an integral equation solution for an inhomogeneous thin sheet representing the upper crust. Their solution is very useful for interpreting geomagnetic and MT data. Ranganayaki and Madden (1980) and Vasseur and Weidelt (1977) also developed inhomogeneous thin sheet solutions.

Recently Das and Verma (1982) and Wannamaker and Hohmann (1983) presented numerical results, based on similar volume integral equation solutions, for a 3D body in a layered earth. The former results are for magnetic dipole excitation and the latter for plane wave excitation. Considerations pertaining to the numerical solution are the same as those described above; the only change is that the dyadic Green's function is more complicated. Wannamaker and Hohmann are able to keep the computer time

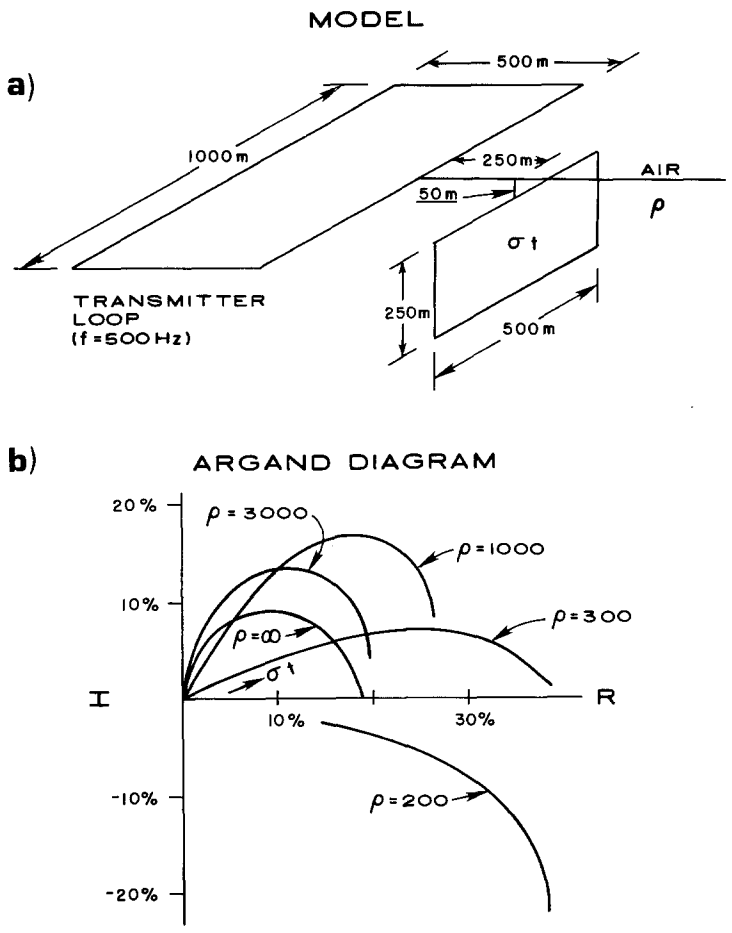

Fig. 5. Response of a thin 3D plate in a conductive half space: (a) Model; (b) Argand diagram for secondary vertical magnetic field as a percent of free-space field, as function of conductivity-thickness of plate and resistivity of half space. Adapted from Lajoie and West (1976).

about the same as for a homogeneous half space host by computing the Hankel transforms on a table and interpolating them during matrix formation.

4. Differential Equation Solutions

Finite difference formulations for 3D scattering have been discussed by Lines and Jones (1973) and by Zhdanov *et al.* (1982). Instead of (15), Lines and Jones approximated the equation

$$\nabla^2 \mathbf{E} - \nabla(\nabla \cdot \mathbf{E}) + k^2 \mathbf{E} = 0, \tag{56}$$

for a plane wave source. Jones and Vozoff (1978) presented MT results based on a finite difference solution of (56).

Zhdanov *et al.* (1982) recommend solving (15) rather than (56) by the finite difference method. Then it is possible to use a 7-point scheme for the finite difference approximation, and, furthermore, the second term in (15) vanishes in regions where conductivity is constant. However, they did not show any 3D numerical results.

Reddy *et al.* (1977) published 3D MT results based on a finite element (FE) solution of (56). They used the Galerkin technique with linear basis and weight functions in hexahedral elements. They alleviated the problem of discontinuous normal electric fields by specifying smooth, rather than abrupt, conductivity boundaries. Thus the second term in (56) results in a volume rather than a surface charge distribution, as in the integral equation approach discussed above. They found that conductivity contrasts greater than 10 result in errors greater than 10% up to three node spacings from a conductivity boundary.

Pridmore *et al.* (1981) presented a 3D FE solution for controlled-source EM applications. They formulated the problem by minimizing a functional, but since the Galerkin approach yields the same equations, that probably is an unnecessary complication. They used tetrahedral elements for the DC problem and hexahedral elements for the EM problem, and, to reduce storage requirements, they solved the system of equations using a point successive over-relaxation method. The optimum over-relaxation factor W is determined by observing the behavior of certain nodal values during iteration. Typically, a DC problem requires 100 iterations, while EM problems require more.

Figure 6 shows a comparison between FE results of Pridmore *et al.* (1981) and results computed using the IE solution described above. The model is a conductive prism 30 m deep with width 30 m, length 120 m, depth extent 90 m, and resistivity 1 ohm-m, which is a standard test model proposed by Braham *et al.* (1978). The transmitter is a fixed vertical magnetic dipole with moment $4\pi A$-m^2 operating at 1000 Hz, and profiles of the secondary vertical magnetic field are shown for half-space resistivities of 30 and 100 ohm-m.

The IE solution, which used 96 cells and did not take advantage of symmetry, took only 5 minutes CPU time on a Univac 1108 computer. By comparison, the FE solution took about 3 hr for 200 iterations, although slightly less accurate results could be calculated in half the time. Since the FE equations are solved iteratively, computations for another transmitter position would require the same amount of computer time. However, IE results for other source positions can be calculated with little additional computer time.

In Figure 6a, the IE and FE results for a conductivity contrast of 30 are in good agreement. However, the agreement deteriorates for a contrast of 100, particularly for the real part of the field, as shown in Figure 6b. As Pridmore *et al.* (1981) show, the agreement is very poor for a contrast of 1000, again especially for the real component.

5. Hybrid Solutions

Three dimensional DE solutions with boundary conditions imposed at great distances

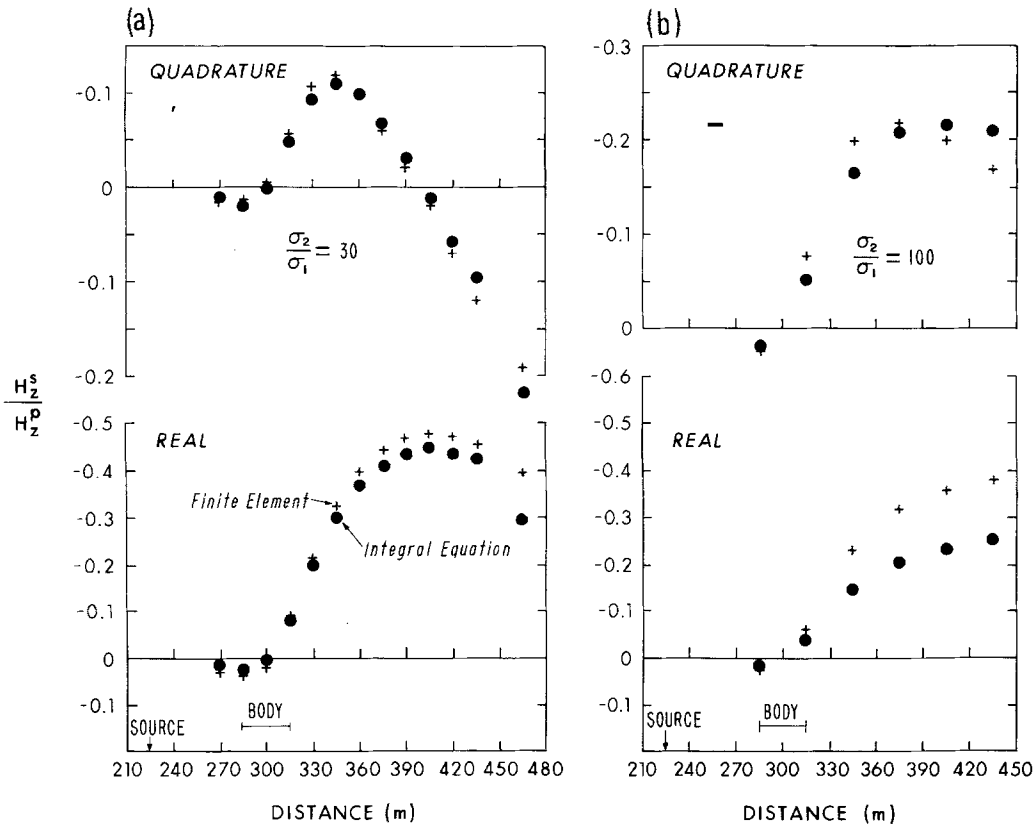

Fig. 6. Comparison between integral equation and finite element results for a 3D conductor in the Earth; (a) $\sigma_b/\sigma_* = 30$, (b) $\sigma_b/\sigma_* = 100$.

have not been very successful. The large grids required result in unreasonable amounts of computer time and storage. Thus recent DE research has focused on hybrid approaches, combining DE and IE solutions, as a means of limiting mesh size.

Finite element discretization of (15) yields a matrix equation for the electric field:

$$\mathbf{L}\mathbf{E} = 0 \tag{57}$$

For either of the hybrid cases shown in Figure 7 we can partition (57) into

$$\begin{bmatrix} \mathbf{L}_{vv} & \mathbf{L}_{vb} \\ \mathbf{L}_{bv} & \mathbf{L}_{bb} \end{bmatrix} \begin{bmatrix} \mathbf{E}_v \\ \mathbf{E}_b \end{bmatrix} = \begin{bmatrix} \mathbf{0} \end{bmatrix}, \tag{58}$$

where subscript v denotes electric fields in the interior (volume) of the mesh, and subscript b denotes electric fields at the boundary nodes. From (58) we can write

$$\mathbf{L}_{vv}\mathbf{E}_v = -\mathbf{L}_{vb}\mathbf{E}_b. \tag{59}$$

However, we can calculate the field on the boundary in terms of the field inside the mesh using (27), which becomes

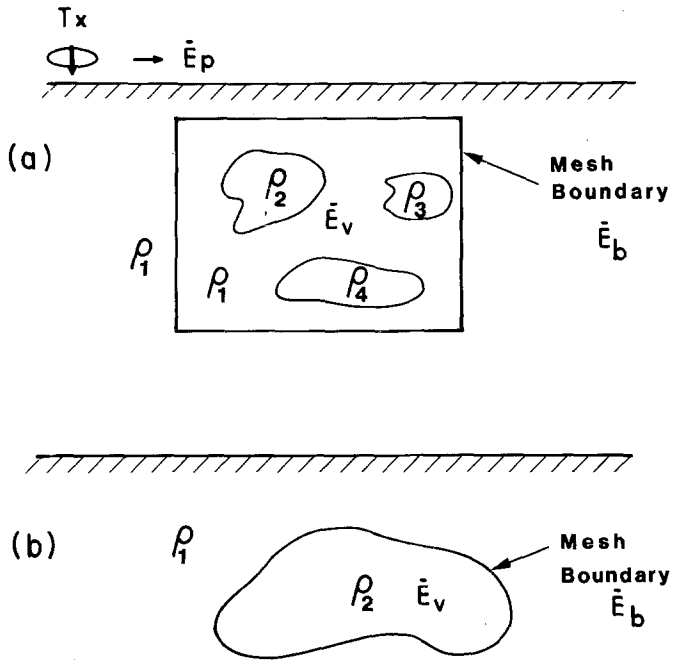

Fig. 7. Geometries for hybrid techniques.

$$\mathbf{E}_b(\mathbf{r}) = \mathbf{E}_b^p(\mathbf{r}) + \int_v \mathcal{G}(\mathbf{r}, \mathbf{r}') \cdot \mathbf{E}_v(\mathbf{r}')\sigma_a(\mathbf{r}')\,dv'. \tag{60}$$

The matrix version of this equation is

$$\mathbf{E}_b = \mathbf{R}\mathbf{E}_v + \mathbf{E}_b^p, \tag{61}$$

where $\mathbf{R}$ is $M \times N$ with M the number of boundary nodes and N the number of interior nodes.

Substituting (61) in (59), we obtain

$$(\mathbf{L}_{vv} + \mathbf{L}_{vb}\mathbf{R})\mathbf{E}_v = -\mathbf{L}_{vb}\mathbf{E}_b^p. \tag{62}$$

In the direct hybrid method (62) is solved for $\mathbf{E}_v$, and then (60) and the corresponding equation for magnetic field are used to calculate the fields outside the mesh. The matrix $\mathbf{L}_{vv} + \mathbf{L}_{vb}$ is full, asymmetric and $N \times N$.

The advantage of the hybrid scheme illustrated in Figure 7a is that the integral in (60) is not singular: $\mathbf{r}$ is never equal to $\mathbf{r}'$. However, the FE solution inside the mesh is plagued by the problem of discontinuous electric fields at conductivity boundaries. On the other hand, for the hybrid scheme of Figure 7b the FE solution operates in a homogeneous region, but evaluation of (60) at singular points on the surface of the mesh is very difficult.

Lee *et al.* (1981), developed an iterative hybrid solution, by assuming an initial guess

for $\mathbf{E}_b$, the boundary field, calculating $\mathbf{E}_v$, then finding a new $\mathbf{E}_b$ using (60), and proceeding iteratively. Their results agree with the FE and IE results shown in Figure 6 for a low-contrast ($\sigma_b/\sigma_* = 30$) model. However, their MT results for a body with a conductivity contrast of 200 do not agree with our IE results as shown by Figures 8 and 9.

Figure 8 compares TM-mode MT apparent resistivity results for a 2D body computed by the FE method with IE results of Wannamaker and Hohmann (1983) and hybrid results of Lee *et al.* (1981) for a 3D body with the same cross section. The body has a conductivity contrast of 200, and the frequency is 0.01 Hz. For this mode of excitation the electric field is perpendicular to strike; thus electric charge on the boundaries of the body, which is required to maintain continuity of normal current, is the main source of the MT response at low frequencies. Since surface charge is included implicity in the 2D formulation for this mode, the 2D and 3D results should be about the same. We have carefully designed our descretization of the 3D body for the IE solution based on convergence checks, and our 3D results are close to the 2D results.

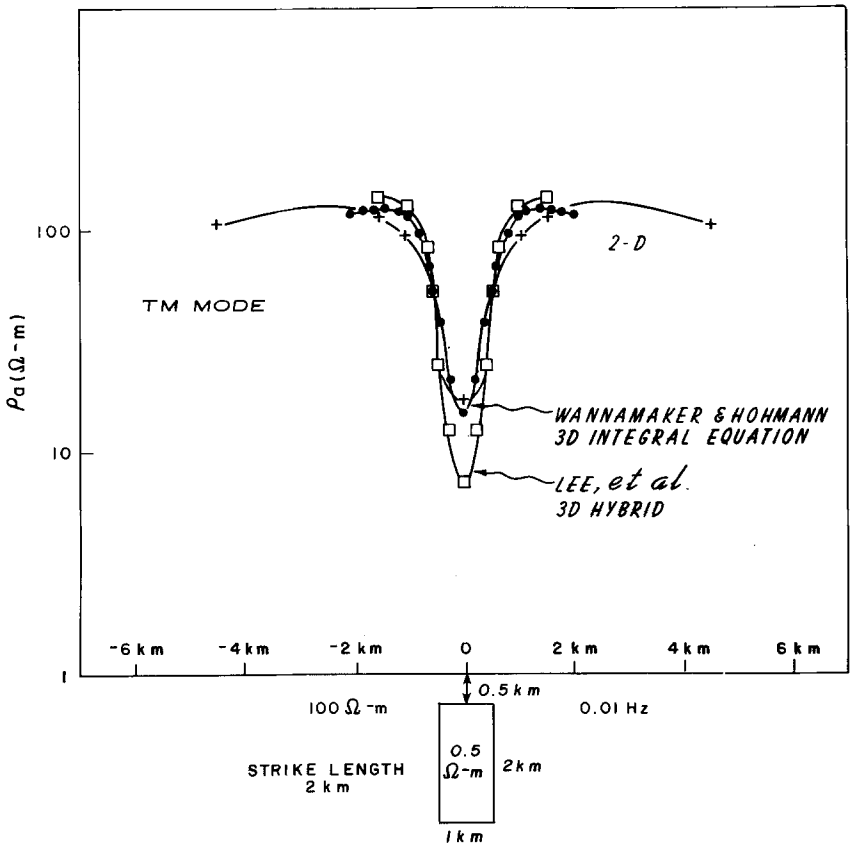

Fig. 8. Comparison of 3D integral equation and hybrid MT results for TM-mode excitation.

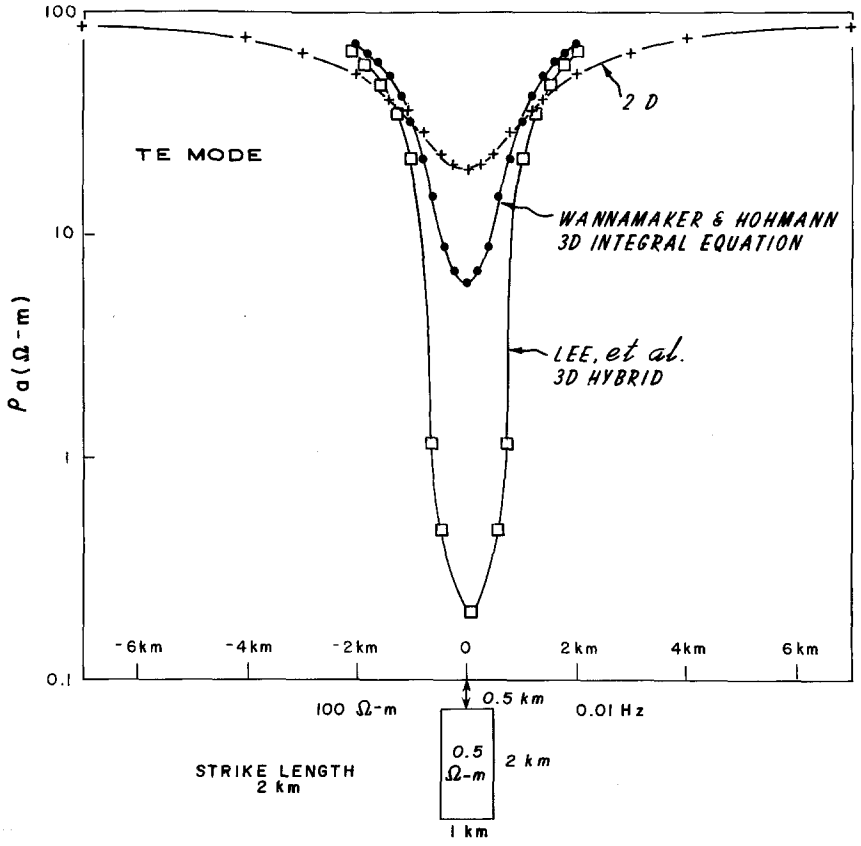

Fig. 9. Comparison of 3D integral equation and hybrid MT results for TE-mode excitation.

The overshoot at the edge of the body in the 3D case is to be expected; it is due to current channeling. The 3D hybrid results of Lee *et al.* (1981) on the other hand, differ considerably from the 2D results over the body.

Figure 9 shows the same comparison for TE excitation, in which case the electric field is parallel to strike, so that there is no surface charge in the 2D case. Since the secondary electric field due to surface charge at the ends of a 3D body is important at low frequencies, it must be very long if its response is to be similar to that of a 2D body. We find that our 3D IE results converge to 2D results as the strike length is increased beyond a skin depth in the host medium. For the short body of Figure 9, the difference between 2D results and our 3D results is to be expected. However, the apparent resistivities computed by Lee *et al.* (1981) appear to be too low.

As shown by Figure 8 and as discussed by Ting and Hohmann (1981), one can interpret TM-mode MT data on a profile over complex elongate 3D models using a 2D finite element or finite difference algorithm. However, TE-mode modeling is of little value, because, charge on the ends of 3D bodies is not taken into account.

6. Time Domain EM Modeling

Transient EM (TEM) techniques have gained widespread acceptance for mineral exploration in the last five years. However, numerical simulation of TEM responses is still in its infancy. Results can be calculated directly in the time domain, or, indirectly, by Fourier transformation of frequency domain results. The former method permits the study of the evolving current system in the earth, a necessity for gaining insight into TEM behavior. However, the latter method probably is more efficient for cases where several transmitter positions are desired. Numerical solutions by both methods are required both for their particular advantages and for validation of results.

6.1. Time stepping solutions

The relevant differential equations, (6), (7), (12), and (13) are initial value problems and they can be solved by time stepping. The spatial variation is approximated by a FE or FD method, and the time derivative is approximated by a finite difference formula. Implicit methods require matrix inversion, while explicit methods do not.

So far, only 2D line-source problems have been solved; in that case the DE, from (6), is

$$\frac{\partial^2 e_y}{\partial x^2} + \frac{\partial^2 e_y}{\partial z^2} - \mu_0 \sigma \frac{\partial e_y}{\partial t} = \mu_0 \frac{\partial j_y^p}{\partial t}. \tag{63}$$

For the usual step current source, the right-hand-side of (63) is an impulse. Kuo and Cho (1980) presented numerical results based on a FE formulation in space and a central difference approximation in time. To achieve stability, they used a Gaussian function for the impulse. They found that their results agreed qualitatively with field data, but they did not show a quantitative check.

We(Oristaglio and Hohmann, 1982) have developed a numerical solution to (63), in which the time derivative of the electric field is approximated by

$$\frac{\partial e_y}{\partial t} = \frac{1}{2\Delta t}(e^{n+1} - e^{n-1}), \tag{64}$$

where nodal values of e_y at $t = n\Delta t$ are denoted by e^n. The spatial derivatives also are approximated by differences. Variable grid spacing is necessary to permit a large enough grid that the analytic solution for a line source can be imposed as the boundary condition in the Earth. For the typical grid point shown in Figure 10, the central difference approximations are:

$$\frac{\partial^2 e_{ij}^n}{\partial x^2} \approx \frac{2}{\Delta x_i + \Delta x_{i+1}}\left(\frac{e_{i+1,j}^n}{\Delta x_{i+1}} + \frac{e_{i-1,j}^n}{\Delta x_i}\right) - \frac{e_{ij}^{n+1} + e_{ij}^{n-1}}{\Delta x_i \Delta x_{i+1}} \tag{65}$$

$$\frac{\partial^2 e_{ij}^n}{\partial z^2} \approx \frac{2}{\Delta z_j + \Delta z_{j+1}}\left(\frac{e_{i,j+1}^n}{\Delta z_{j+1}} + \frac{e_{i,j-1}^n}{\Delta z_j}\right) - \frac{e_{ij}^{n+1} + e_{ij}^{n-1}}{\Delta z_j \Delta z_{j+1}}, \tag{66}$$

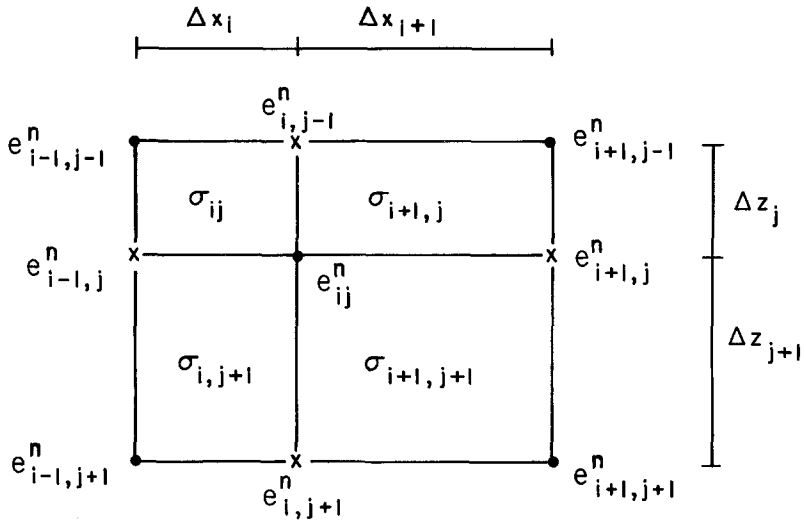

Fig. 10. Typical grid point for 2D finite difference time domain solution.

where, following Dufort and Frankel (1953), we have replaced the electric field at the central point at time $n\Delta t$ by

$$e_{ij}^n = \tfrac{1}{2}(e_{ij}^{n+1} + e_{ij}^{n-1}), \tag{67}$$

which, remarkably, yields a scheme that is both explicit and unconditionally stable. The conductivity is taken as a typical weighted average (Brewitt-Taylor and Weaver, 1976).

Since the field in the air satisfies Laplace's equation, the grid can be terminated at the earth's surface using upward continuation, which is another advantage of an explicit method, in addition to the absence of matrix inversion.

The TEM integral equation corresponding to (27) in the frequency domain is

$$\mathbf{e}(\mathbf{r}, t) = \mathbf{e}_p(\mathbf{r}, t) + \int_v \int_0^t \mathbf{g}(\mathbf{r}, \mathbf{r}'; t - t') \cdot \mathbf{e}(\mathbf{r}', t)\sigma_a(\mathbf{r}', t')\sigma_a(\mathbf{r}')\,\mathrm{d}t'\,\mathrm{d}v', \tag{68}$$

where, for a whole space, e.g., the dyadic Green's function is derived using the time domain version of (23):

$$\mathbf{e}^s = -\mu_0 \frac{\partial \mathbf{a}}{\partial t} - \nabla\varphi, \tag{69}$$

with, from (24) and (25)

$$\mathbf{a}(\mathbf{r}) = \int_v \mathbf{j}_s(\mathbf{r}')g(\mathbf{r}, \mathbf{r}')\,\mathrm{d}v', \tag{70}$$

and

$$\varphi(\mathbf{r}) = \frac{1}{\sigma_*} \int_v \nabla \cdot \mathbf{j}_s(\mathbf{r}') g(\mathbf{r}, \mathbf{r}') \, dv'. \tag{71}$$

The time domain scalar Green's function $g(\mathbf{r}, \mathbf{r}')$, obtained by inverse Fourier transforming (26) is:

$$g(\mathbf{r}, \mathbf{r}') = (\mu_0 \sigma_*)^{1/2} \frac{\exp[-(\mu_0 \sigma_* |\mathbf{r} - \mathbf{r}'|)^2/4t]}{8\pi^{3/2} t^{3/2}}. \tag{72}$$

Other terms must be added to account for the earth-air interface and any other horizontal layers.

6.2. Transformation of Frequency Domain Results

The frequency domain system function $H(\omega)$ for an electromagnetic field component and the time domain impulse response $h(t)$ for the same component are related by the transform pair

$$H(\omega) = \int_0^\infty h(t) e^{-i\omega t} \, dt \tag{73}$$

and

$$h(t) = \frac{1}{2\pi} \int_{-\infty}^{\infty} H(\omega) e^{i\omega t} \, d\omega, \tag{74}$$

since the impulse response is causal.

Although the inverse Fourier transform can be approximated by a discrete Fourier transform using an FFT algorithm, the number of frequency domain data points necessary for accurate estimation of $h(t)$ is large and their calculation is expensive. As Lamontagne (1975) has observed, simple interpolation of a sparse set of $H(\omega)$ values does not solve the problem; the discrete inverse Fourier transform of interpolated field values is sensitive to the particular interpolant used, and the calculated impulse response is usually not causal.

These problems can be circumvented by treating (73) as an inverse problem for $h(t)$ and utilizing the powerful stabilizing techniques of geophysical inversion theory, as shown by Lamontagne (1975). In a more recent work, Tripp (1982) shows that the impulse response can be written in terms of a decay spectrum $A(k)$:

$$h(t) = \int_0^\infty A(k) e^{-kt} \, dk. \tag{75}$$

Thus we can solve (73), a Fredholm integral equation of the first kind, by the method of moments, utilizing exponential basis functions and delta weight functions. We approximate $h(t)$ by

$$\hat{h}(t) = \sum_{n=1}^{N} A_n e^{-k_n t}, \tag{76}$$

where k_n is the nth decay constant (reciprocal of the time constant). Substituting (76) in (73) yields

$$H(\omega) = \sum_{n=1}^{N} \frac{A_n}{k_n + i\omega}. \tag{77}$$

Incorporating delta weight functions

$$w_m(\omega) = \delta(\omega - \omega_m)$$

gives

$$\sum_{n=1}^{N} \frac{1}{k_n + i\omega_m} A_n = H(\omega_m). \tag{78}$$

Writing (78) for each of the M values of m yields a matrix equation

$$\mathbf{KA} = \mathbf{H}$$

for determining the N values of A_n. Then the impulse response is given by (76), and the response for any transmitter wave form is given by convolution.

Tripp (1982) discusses the solution of (73) in detail. In general, N must be greater than M, and, since (73) is ill-posed, a generalized inverse or ridge regression solution is required. For many cases, ten frequency domain values are sufficient.

Figure 11 shows a check between 2D time domain results obtained by inverse Fourier transforming integral equation results (Hohmann, 1975) and results calculated by the direct time domain finite difference solution of Oristaglio and Hohmann (1982). Line sources of current simulate the front and back of a large horizontal loop at the surface of the earth, and profiles over a conductive body are shown for four delay times. Plotted is the vertical magnetic field impulse response, which is equivalent to the time derivative of the step response. The latter is approximately what is measured by many practical systems. Note the migration of the vertical field cross-over back toward the body at later times as the currents in the body become more important relative to the half-space currents.

The agreement between the two solutions is good. For the frequency domain calculations, the sampled frequencies ranged from 0.1 to 1000 Hz, and the cross section of the body was divided into square cells with edges shorter than one skin depth in the body. The finite difference solution used 20-m cells near the body, with the cell size gradually increasing to 400 m at the boundary of the grid. The time steps were 0.1 μs for the first 1000 iterations, 1 μs for the next 400 iterations, and 2 μs for the last 17 000 iterations, which carried the solution out to 35 ms.

Recent work indicates that similar results can be computed with much less computer time if one solves for the secondary field using the equation:

$$\frac{\partial^2 e_y^s}{\partial x^2} + \frac{\partial^2 e_y^s}{\partial z^2} - \mu_0 \sigma \frac{\partial e_y^s}{\partial t} = \mu_0 \sigma_a \frac{\partial e_y^p}{\partial t} \tag{79}$$

rather than for the total field using (63). Since the source is a smoother function of time

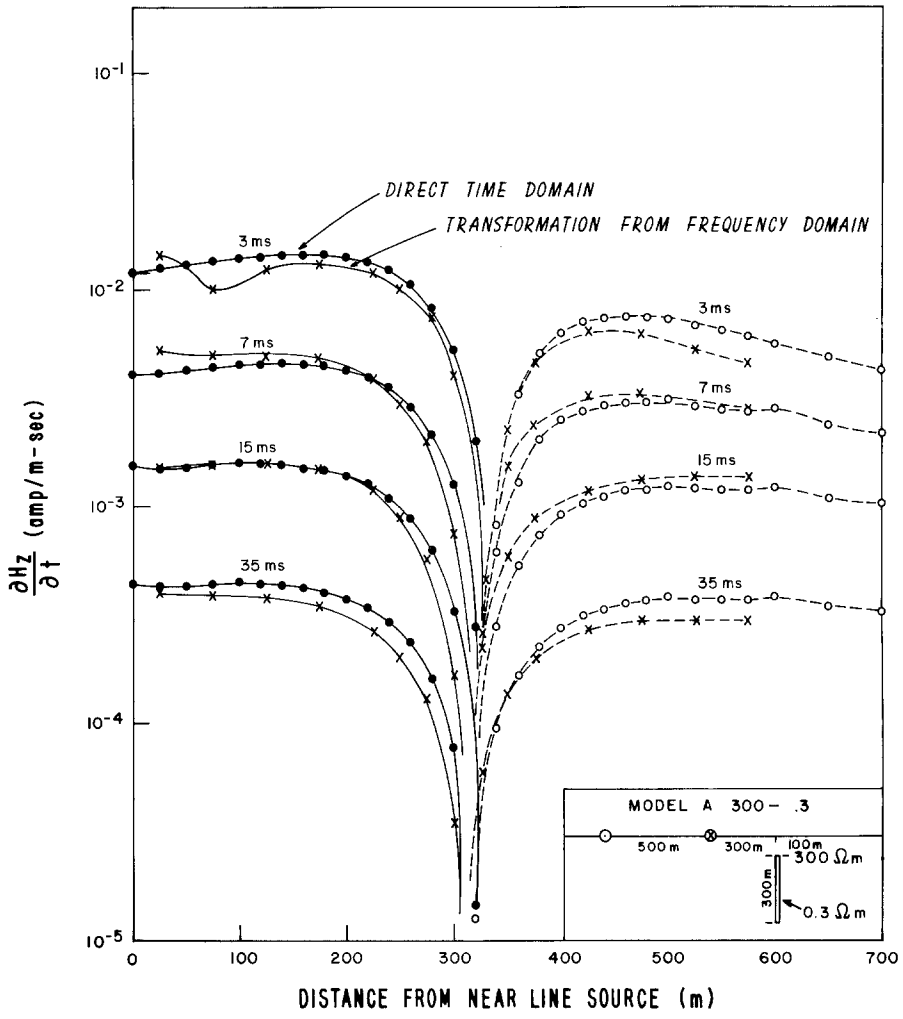

Fig. 11. Comparison between 2D time domain EM results computed by time stepping and by inverse Fourier transformation.

and the secondary field is a smoother spatial function at the earth's surface, one can use larger time steps and coarser spatial discretization.

Annan (1974) developed an elegant method of calculating the frequency and time domain EM responses of a thin 3D plate in free space. Classically the response of a body whose surface coincides with a constant-coordinate surface, such as a sphere , is calculated in terms of analytic eigenfunctions, with no numerical solution required. Each mode in the eigenfunction expansion is decoupled from the other modes, so that the impedance matrix is diagonal. In contrast, for bodies of arbitrary shape, the impedance matrix for the IE numerical solution links the expansion function coefficients for the scattering currents with those for the primary electric field by a full matrix.

By diagonalizing the IE impedance matrix, Annan formulated a solution for a general body in terms of real eigencurrents expanded in the full-range expansion functions of his numerical solution. He found that for a body in free space the eigencurrent geometries are the same for all frequencies, and that each eigencurrent has the same frequency response as that of a simple loop circuit. Thus each mode contributes a single exponential decay in the time domain, and it is easy to calculate TEM responses by summing the decays for the first few modes.

Tripp (1982) investigated a similar modal solution for a body in a conductive half space. He found that the eigencurrent patterns change with frequency, so that the modal solution has no advantage over a direct numerical solution. However, it still may be possible to formulate the problem in terms of complex modes that diagonalize the impedance matrix and that simplify calculations.

Finally, Lee (1981) calculated the TEM response of a sphere in a layered earth by inverse Fourier transforming IE results. However, no TEM solution for general 3D bodies has yet been developed.

7. Summary

Progress in 3D EM modeling has been slow but steady over the last ten years. Integral equation solutions have been the most successful, and they have been improved by incorporating symmetry using group theory and by using a vector-scalar potential formulation for computing matrix elements. However, hybrid techniques, wherein finite element grids are reduced in size by computing boundary values by integrating over interior fields, appear promising. Thin-sheet simplifications have provided much insight, both for EM prospecting and for crust-mantle studies.

Much more research is needed, however. Frequency domain numerical solutions for 3D bodies in a conductive earth are limited to low conductivity contrasts and simple bodies. Although transient EM (TEM) methods are becoming increasingly popular, numerical solutions for general models have only been developed for the 2D case. I hope that the discussion in this paper will stimulate interest in 3D TEM modeling.

References

Annan, A. P.; 1974, 'The Equivalent Source Method for Electromagnetic Scattering Analysis and its Geophysical Application', Ph. D. Thesis, Memorial University of Newfoundland, 242 p.

Braham, B., Haren, R., Lappi, D., Lemaire, H., Payne, D., Raiche, A., Spies, B., and, Vozoff, K.: 1978, 'Lecture Notes from the U.S.-Australia Electromagnetic Workshop', *Bull. Aust. Soc. Explor. Geophys.* **9**, 2–33.

Brewit-Taylor, C. R. and Weaver, J. T.: 1976, 'On the Finite Difference Solution of Two-Dimensional Induction Problems', *Geophys. J. Roy. Astron. Soc.* **47**, 375–396.

Butler, C. M. and Wilton, D. R.: 1975, 'Analysis of Various Numerical Techniques Applied to Thin-Wire Scatterers', *IEEE Trans. on Ant. and Prop.*, AP-23, 534–540.

Das, U. C. and Verma, S. K.: 1982, 'Electromagnetic Response of an Arbitrary Shaped Three-Dimensional Conductor in a Layered Earth-Numerical Results', *Geophys. J. Roy. Astron. Soc.* **68**, 55–56.

Dawson, T. W. and Weaver, J. T.: 1979, 'Three-Dimensional Induction in a Non-Uniform Thin Sheet at the Surface of a Uniformly Conducting Earth', *Geophys. J. Roy. Astron. Soc.* **59**, 445–462.

DuFort, E. C. and Frankel, S. P.: 1953, 'Stability Conditions in the Numerical Treatment of Parabolic Differential Equations', *Math. Tables and Other Aids to Comp.* (now, *Math. of Comp.*), 7, 135–152.

Harrington, R. F.: 1968, *Field Computation by Moment Methods*, Krieger, Melbourne, Florida, 229 p.

Hohmann, G. W.: 1975, 'Three-Dimensional Induced Polarization and Electromagnetic Modeling', *Geophysics* **40**, 309–324.

Jones, F. W. and Thompson, D. J.: 1974, 'A Discussion of the Finite Difference Method in Computer Modeling of Electrical Conductivity Structures', *Geophys. J. Roy. Astron. Soc.* **37**, 537–543.

Jones, F. W. and Vozoff, K.: 1978, 'The Calculation of Magnetotelluric Quantities for Three-Dimensional Conductivity Inhomogeneities', *Geophysics* **43**, 1167–1175.

Kuo, J. T. and Cho, Vong-heng: 1980, 'Transient Time-Domain Electromagnetics', *Geophysics* **45**, 271–291.

Lajoie, J. J. and West, G. F.: 1976, 'The Electromagnetic Response of a Conductive Inhomogeneity in a Layered Earth', *Geophysics* **41**, 1133–1156.

Lamontagne, Y.: 1975, 'Applications of Wideband, Time-Domain Electromagnetic Measurements in Mineral Exploration', Ph. D. Thesis, University of Toronto, 329 p.

Lee, T. J.: 1981, 'Transient Electromagnetic Response of a Sphere in a Layered Medium', *PAGEOPH* **119**, 309–338.

Lee, K. H., Pridmore, D. F., and Morrison, H. F.: 1981, 'A Hybrid Three-Dimensional Electromagnetic Modeling Scheme', *Geophysics* **46**, 796–805.

Lines, L. R. and Jones, F. W.: 1973, 'The Perturbation of Alternating Geomagnetic Fields by Three-Dimensional Island Structures', *Geophys. J. Roy. Soc.* **32**, 133–154.

Meyer, W. H.: 1976, 'Computer Modelling of Electromagnetic Prospecting Methods', Ph. D. Thesis, University of California, Berkeley, 155 p.

Miller, E. K. and Deadrick, F. J.: 1975, 'Some Computational Aspects of Thin Wire Modeling', in R. Mittra (ed.), *Numerical and Asymptotic Techniques in Electromagnetics*, New York, Springer-Verlag, 260 p.

Oristaglio, M. L. and Hohmann, G. W.: 1982, *Numerical Solution of Maxwell's Equations in the Time Domain*, Technical Program Abstracts and Biographes, Society of Exploration Geophysicists, 1982 Annual Meeting.

Pridmore, D. F., Hohmann, G. W., Ward, S. H., and Sill, W. R.: 1981, 'An investigation of Finite-Element Modeling for Electrical and Electromagnetic Data in Three Dimensions', *Geophysics* **46**, 1009–1024.

Raiche, A. P.: 1974, 'An Integral Equation Approach to 3D Modeling', *Geophys. J. Roy. Astron. Soc.* **36**, 363–376.

Ranganayaki, R. P. and Madden, T. R.: 1980, 'Generalized Thin Sheet Analysis in Magnetotellurics: An Extension of Price's Analysis', *Geophys. J. Roy. Astron. Soc.* **60**, 445–457.

Reddy, I. K., Rankin, D., and Philips, R. J.: 1977, 'Three-Dimensional Modeling in Magnetotelluric and Magnetic Variational Sounding', *Geophys. J. Roy. Astron. Soc.* **51**, 313–325.

Ting, S. C. and Hohmann, G. W.: 1981, 'Integral Equation Modeling of Three-Dimensional Magnetotelluric Response', *Geophysics* **46**, 182–197.

Tripp, A. C.: 1982, 'Multi-Dimensional Electromagnetic Modeling', Ph. D. Thesis, University of Utah, 179 p.

Tripp, A. C. and Hohmann, G. W.: 1983, 'Block Diagonalization of the Electromagnetic Impedance Matrix of a Symmetric Buried Body Using Group Theory', *IEEE Trans. Geoscience and Remote Sensing*, (in press).

Vasseur, G. and Weidelt, P.: 1977, 'Bimodal Electromagnetic Induction in Non-Uniform Thin Sheets with an Application to the Northern Pyrenean Induction Anomaly', *Geophys. J. Roy. Astron. Soc.* **51**, 669–690.

Wannamaker, P. E. and Hohmann, G. W.: 1983, 'Electromagnetic Modeling of Three-Dimensional Bodies in Layered Earths Using Integral Equations', *Geophysics* (in press).

Weidelt, P.: 1975, 'Electromagnetic Induction in Three-Dimensional Structures', *J. Geophys.* **41**, 85–109.

Zhdanov, M. S., Golubev, N. G., Spichak, V. V., and Varentsov, Iv. M.: 1982, 'The Construction of Effective Methods for Electromagnetic Modelling', *Geophys. J. Roy. Astron. Soc.* **68**, 589–607.